RESEARCH

The aggressiveness of succinate dehydrogenase subunit B-deficient chromaffin cells is reduced when their bioelectrical properties are restored by glibenclamide

Francesca Amore[1], Rachele Garella[2], Alice Santi[1], Daniele Guasti[3], Serena Martinelli[1,4,5], Letizia Canu[1,4,5], Daniele Bani[3], Jiri Neuzil[6,7,8], Mario Maggi[1,4,5], Roberta Squecco[2] and Elena Rapizzi[2,4,5]

[1]Department Experimental and Clinical Biomedical Sciences, University of Florence, Florence, Italy
[2]Department Experimental and Clinical Medicine, University of Florence, Florence, Italy
[3]Department of Experimental and Clinical Medicine, Imaging Platform, University of Florence, Italy
[4]Centro di Ricerca e Innovazione sulle Patologie Surrenaliche, AOU Careggi, Florence, Italy
[5]ENS@T Center of Excellence, Florence, Italy
[6]Institute of Biotechnology, Czech Academy of Sciences, Prague-West, Czech Republic
[7]School of Pharmacy and Medical Science, Griffith University, Southport, Queensland, Australia
[8]Faculty of Science and 1st Medical Faculty, Charles University, Prague, Czech Republic

Correspondence should be addressed to E Rapizzi: elena.rapizzi@unifi.it

*(F Amore and R Garella contributed equally to this work)

Abstract

Pheochromocytomas/paragangliomas (PPGLs) are neuroendocrine tumours, mostly resulting from mutations in predisposing genes. Mutations of succinate dehydrogenase (SDH) subunit B (SDHB) are associated with high probability of metastatic disease. Since bioelectrical properties and signalling in cancer are an emerging field, we investigated the metabolic, functional and electrophysiological characteristics in human succinate dehydrogenase subunit B (SDHB)-deficient pheochromocytoma cells. These cells exhibited reduced SDH function with elevated succinate-to-fumarate ratio and reduced intracellular ATP levels. The analysis of membrane passive properties revealed a more hyperpolarized membrane potential and a lower cell capacitance of SDHB-deficient cells compared to the parental ones. These bioelectrical changes were associated with reduced proliferation and adhesion capacity of SDHB-deficient cells. Only in SDHB-deficient cells, we also observed an increased amplitude of potassium currents suggesting an activation of ATP-sensitive potassium channels (K_{ATP}). Indeed, exposure of the SDHB-deficient cells to glibenclamide, a specific K_{ATP} inhibitor, or to ATP caused normalization of potassium current features and altered proliferation and adhesion. In this work, we show for the first time that reduced intracellular ATP levels in SDHB-deficient chromaffin cells impaired cell bioelectrical properties, which, in turn, are associated with an increased cell aggressiveness. Moreover, we first ever demonstrated that glibenclamide not only reduced the outward potassium currents in SDHB-deficient cells but increased their growth capacity, reduced their ability to migrate and shifted their phenotype towards one more similar to that of parental one.

Key Words

- pheochromocytoma/paraganglioma
- succinate dehydrogenase
- bioelectrical properties
- ATP-sensitive potassium channels
- glibenclamide

Endocrine-Related Cancer (2023) **30**, **e230167**

https://erc.bioscientifica.com
https://doi.org/10.1530/ERC-23-0167

Introduction

Pheochromocytomas/paragangliomas (PPGLs) are rare catecholamine-secreting neuroendocrine tumours arising from the adrenal medulla or the extra-adrenal paraganglia. These tumours are characterized by a large spectrum of hereditary predispositions; however, some of them occur sporadically. About 70% of PPGLs are associated with germline or somatic mutations in almost 20 susceptibility genes known so far, which is the highest rate among all tumour types (Buffet *et al.* 2020, Dariane *et al.* 2021, Jhawar *et al.* 2022). These genes include those encoding the four subunits of succinate dehydrogenase (SDH) (SDH subunit A (SDHA), SDH subunit B (SDHB), SDH subunit C (SDHC) and SDH subunit D (SDHD)). PPGLs are predominantly non-metastatic, and surgery is the most frequent treatment; however, in the presence of metastases, resection is not possible and prognosis is limited. SDHB germline mutations are considered to be among predominant risk factors associated with metastatic evolution (Buffet *et al.* 2020, Dariane *et al.* 2021). However, specific mechanisms by which the impaired SDH activity leads to tumourigenesis and why the loss of SDHB subunit specifically predisposes to a more aggressive phenotype remain uncertain.

The SDH complex is located in the inner mitochondrial membrane, where it catalyses oxidation of succinate to fumarate as part of the tricarboxylic acid cycle (TCA) and reduction of ubiquinone to ubiquinol as part of oxidative phosphorylation (OXPHOS). Tumour tissue analysis has demonstrated that inhibition of SDH activity induces intracellular accumulation of succinate (Richter *et al.* 2014) – that acts as an oncometabolite (Tretter *et al.* 2016) – and OXPHOS dysfunction (Fliedner *et al.* 2012), leading to reduced levels of ATP, ADP and AMP (Rao *et al.* 2013). It has been recently shown that the loss of SDHB in human pheochromocytoma hPheo1 cells causes a significant decrease in basal respiration (Matlac *et al.* 2021).

In the context of metabolic changes, ATP-sensitive potassium (K_{ATP}) channels are of special interest, because their opening depends on the metabolic state of a cell. They close when the ATP/ADP ratio is high and open when it is low (Wang *et al.* 2022). K_{ATP} channels thus provide a link between changes in metabolism and membrane bioelectrical activity. Furthermore, bioelectricity is a key feature mediating multiple cellular processes. For instance, the resting membrane potential (RMP) – that represents the voltage across a membrane due to the equilibrium of extracellular and intracellular ion concentrations – is a crucial modulator of cell behaviour, regulating important cell functions such as proliferation and differentiation (Sundelacruz *et al.* 2009). However, the relation between RMP and these functions is rather complex since RMP reflects the overall activity of several ion channels. Among these, K^+ channels are recognized as key players of proliferation and cell cycle progression (Dubois & Rouzaire-Dubois 1993, MacFarlane & Sontheimer 2000). In addition, besides the voltage-dependent ion channel activation, other mechanisms may contribute to the control of RMP, such as stretch-activated channels (Formigli *et al.* 2007, Sbrana *et al.* 2008, Aydar *et al.* 2009), ionic pumps (Na^+/K^+ ATPase and Ca^{2+} ATPase), Na^+/Ca^{2+} exchanger (Becchetti 2011) and voltage-independent channels such as IKCa and K_{ATP} (Abdul *et al.* 2003, Blackiston *et al.* 2009, Haren *et al.* 2010). K_{ATP} channels indeed mediate the electrical transduction of the metabolic state of the cell by coupling cellular metabolism to the RMP (Nichols 2006).

Given that chromaffin cells are neuroendocrine cells and given that biophysical properties are key features in these cells, we investigated the metabolic, functional and electrophysiological characteristics of parental (Ghayee *et al.* 2013) and SDHB-deficient hPheo1 cells (Matlac *et al.* 2021).

Materials and methods

Cell culture and materials

hPheo1 cells (parental wild type and the knockout for the SDHB subunit, hereinafter referred to as parental and SDHB deficient, respectively), generated by Ghayee and Matlac (Ghayee *et al.* 2013, Matlac *et al.* 2021) and kindly provided by Jiri Neuzil, were maintained at 5% CO_2, 37°C in RPMI supplemented with 10% foetal bovine serum (FBS), with 4.5 g/L glucose, 2 mM L-glutamine, 100 U/mL of penicillin/streptomycin, 2 mM of sodium pyruvate and 50 µg/mL uridine (complete RPMI). Glibenclamide was purchased from Sigma (Sigma-Aldrich) and was dissolved in dimethyl sulfoxide (DMSO).

Proliferation assay

To evaluate proliferation, cells were seeded at the density of 2.5×10^4 per well into 12-well plates, allowed to adhere overnight and then treated or not with increasing doses of glibenclamide (30 nM, 300 nM, 100 nM, 1 µM, 3 µM, 10 µM, 33 µM and 100 µM) in complete culturing medium for 6 days.

https://erc.bioscientifica.com
https://doi.org/10.1530/ERC-23-0167

SDH activity

Cell homogenates (50 µg) were incubated in a phosphate buffer containing sodium azide, 2,6 dichlorophenolindophenol (DCPIP), sodium succinate, and phenazine methosulphate. Complex II specific activity was evaluated by photometry using the Victor3 1420 Multilabel Counter (Packard Instruments, PerkinElmer, Waltham MA, USA) to measure the decrease in absorbance that resulted from the oxidation of DCPIP at 600 nm (Rapizzi *et al.* 2015).

Western blotting

Cells were lysed in a buffer containing 50 mM Tris–HCl, pH 7.5, 120 mM NaCl, 1 mM EGTA, 6 mM EDTA, 15 mM $Na_4P_2O_7$, 20 mM NaF, 1% Triton X-100 and protease inhibitor cocktail. Lysates were clarified by centrifugation at 10,000 ***g*** for 15 min at 4°C, and supernatants were quantified for protein content (Coomassie Blue reagent, Bio-Rad). All passages were carried out on ice as previously described (Rapizzi *et al.* 2014). Proteins (20 µg) were separated using 10% or 12% sodium dodecyl sulphate polyacrylamide (SDS-PAGE) gels and transferred to PVDF membranes (Fisher Scientific or Immobilon, Millipore, MA, USA). Proteins with bound antibodies were detected using the ECL reagent (Immobilon Crescendo, Millipore, MA, USA) and analysed with the Bio-Rad ChemiDoc Imaging System (Quantity One). Band intensity was determined by optical density analysis using the image J software. The polyclonal anti-SDHB IgG and anti-SDHD IgG were from Sigma-Aldrich (HPA002868 and SAB3500797, respectively), anti-monocarboxylate transporter 4 (MCT4) IgG was from Santa Cruz Biotechnology (sc-50329), anti-$K_{ir}6.1$ IgG was from Alomone Labs (Jerusalem, Israel) (APC-105). The monoclonal anti-monocarboxylate transporter 1 (MCT1) IgG was from GeneTex (Irvine, CA, USA) (GTX631643), anti-SDHA IgG antibody was from Abcam (Cambridge, United Kingdom) (ab14715), anti-actin IgG and anti-GAPDH IgG, both used as housekeeping proteins, were from Santa Cruz Biotechnology (SC-1615) and Sigma-Aldrich (G8796), respectively. Secondary anti-mouse and anti-rabbit and IgGs were from Santa Cruz Biotechnology (sc-516102, sc-2357, sc-2354, respectively).

Gas chromatography–mass spectrometry

Intracellular succinate-to-fumarate ratio and lactate levels were evaluated by means of gas chromatography–mass spectrometry (GC-MS). Briefly, 5 × 10^5 cells were collected and subjected to extraction using a mixture of MeOH:H_2O (4:1) containing 1 µg/mL of norvaline, used as internal standard. Samples were sonicated and centrifuged at 15,000 ***g***. for 10 min at 4°C The supernatant was collected, and dried polar metabolites were derivatized with 10 µL of methoxyamine hydrochloride in pyridine (40 mg/mL) (Sigma-Aldrich) at 37°C for 1.5 h. Then, 50 µL of *N*-tert-butyldimethylsilyl-*N*-methyltrifluoroacetamide with 1% tert-butyldimethylchlorosilane (Sigma-Aldrich) were added and samples were incubated at 60°C for 30 min. Samples were acquired on an Intuvo 9000 GC System 5977B MSD (Agilent Technologies). Sample (1 µL) was injected into a HP-5MS UI GC column in splitless mode using an inlet temperature of 240°C. GC runs were performed with helium as carrier gas at 1.1 mL/min. The GC oven temperature ramp was from 70°C to 280°C. The first temperature ramp was from 70°C to 140°C at 3°C/min. The second temperature ramp was from 140°C to 150°C at 1°C/min. The third temperature ramp was from 150°C to 280°C at 3°C/min. The measurement of metabolites was performed under electron impact ionization at 70 eV using a SIM mode. The ion source and transfer line temperatures were set to 230°C and 290°C, respectively. For the determination of relative metabolite abundances, the integrated signal of selected ions for each metabolite was normalized by the signal from norvaline and cell protein content.

Extracellular pH and lactate measurement

Cells were seeded into a 6-well plate with a density of 7.5 × 10^4 per well in complete RPMI. After 72 h, culture media were harvested, and their pH was immediately assessed by pH meter (Basic 20 pH, Crison, Barcelona, Spain). pH of RPMI medium was used as control (Ctr). For lactate measurements, Lactate Colorimetric/Fluorometric Assay Kit (Abcam, Cambridge, UK) was used, according to the manufacturer's protocol. Briefly, culture media were centrifugated at 4°C, 14,000 ***g*** for 15 min, then 2 µL/each sample in triplicates were mixed with 48 µL of Buffer and 50 µL of mix solution in a 96-well plate, and left at RT for 30 min. The absorbance was measured at 570 nm wavelength using a microplate reader VICTOR³ 1420 Multilabel Counter (Packard Instruments, Perkin-Elmer, Waltham, MA, USA) and normalized on cell number.

Intracellular ATP measurement

For intracellular ATP evaluation, we used the CellTiter-Glo luminescent cell viability assay (Promega Corporation,

https://erc.bioscientifica.com
https://doi.org/10.1530/ERC-23-0167

Madison, WI, USA) performed according to the manufacturer's protocol as described (Martinelli *et al.* 2022). Briefly, tumour cells were seeded into 96-well plates at the density of 2.5×10^4 per well. After 24 h, triplicates for each cell line were counted and used for normalization. In other three wells for each cell line, cells were washed twice in phosphate-buffered saline (PBS) and 125 µL of CellTiter-Glo and 125 µL of PBS were added into each well. The culture plates were gently shaken and incubated at room temperature for 30 min to stabilize the luminescent signal. Luminescence was measured using the Victor³ 1420 Multilabel Counter (Packard Instruments, Perkin-Elmer, Waltham, MA, USA).

Electron microscopy

Cells were pelleted by centrifugation, washed with PBS and fixed in cold 2.5% glutaraldehyde and 2% formaldehyde in 0.1 M sodium cacodylate buffer (pH 7.4) overnight at 4°C and post-fixed in cold 1% osmium tetroxide in 0.1 M phosphate buffer (pH 7.4) for 1 h at room temperature. The samples were dehydrated in graded acetone, passed through propylene oxide and embedded in epoxy resin (Epon 812). Ultrathin sections were stained with gadolinium acetate and alkaline bismuth sub-nitrate and examined by means of the JEM 1010 electron microscope (Jeol, Tokyo, Japan) at 80 kV. Micrographs were taken with the Veleta Radius (EMSIS, Muenster, Germany) digital camera connected to a personal computer with dedicated software (RADIUS EMSIS, Muenster, Germany).

Computational analysis of mitochondria and mitochondrial cristae areas and perimeters was performed using iTem Soft Imaging System Program. Briefly, the edges of mitochondria and cristae were carefully and faithfully drawn by hand, then values of the areas and perimeters were automatically calculated by the program itself.

Quantitative real time-polymerase chain reaction (qRT)-PCR

The extraction of total RNA from hPheo1 Parental and SDHB-deficient cells was performed with TRIzol reagent (Life Technologies) and RNeasy Mini Kit (Qiagen), both according to the manufacturers' indications. RNA concentration and quality were measured with a Nanodrop ND-1000 (Thermo Fisher Scientific) at 260 and 280 nm. Absorbance ratios were between 2.0 and 2.1 for all samples. cDNA synthesis was carried out with the iScript cDNA Synthesis Kit (Bio-Rad Laboratories) and 100 ng of mRNA in 20-µL reaction volume, in accordance with the following protocol: 5 min at 25°C, 30 min at 42°C and 5 min at 85°C. Semiquantitative RT-PCR amplification and detection were carried out with the SsoAdvanced Universal Probes Supermix and the CFX96 Two-Color Real-Time PCR Detection System (Bio-Rad Laboratories) with the following thermal cycler conditions: 40 cycles at 95°C for 15 s and 60°C for 1 min. Gene expression analysis was performed with predeveloped assays purchased from Life Technologies (in Table 1, we report the assay list and probe IDs). The 18S ribosomal RNA subunit was quantified with a predeveloped assay and used as the housekeeping gene for the relative quantitation of the target genes based on a slight modification of the comparative threshold cycle $2^{-\Delta\Delta Ct}$ method (Livak & Schmittgen 2001).

Trypsin sensitivity test and adhesion assay

Cells were plated in a 12-well plate at the density of 2×10^4. After 24 h, cells were treated or not with increasing doses of glibenclamide (30 nM, 1 µM, 3 µM) in a complete culturing medium for 72 h.

For trypsin sensitivity, cells were washed twice in PBS and treated with 0.05% w/v trypsin (Euroclone, Milan, Italy) for 1 min. The detached cells were recovered, counted and normalized to a total cell number (Rossitti *et al.* 2020).

For the adhesion assay, cells were harvested and seeded in 96-well plates at the density of 1×10^4 per well. After 4 h, non-adherent cells were discarded and the remaining cells stained for 5 min with Bengal rose (0.25% in PBS, pH 7.3). After two washing steps with PBS, cells were lysed with PBS/ethanol (1:1) for 30 min under continuous shaking. Lysates were then transferred in a 96-well plate and absorption was evaluated by Victor³ 1420 Multilabel Counter (Packard Instruments, Perkin-Elmer) at 560 nm. PBS/ethanol (1:1) was used as blank (Luciani *et al.* 2013).

Table 1 Predeveloped assays and relative IDs.

Human assay	IDs
Snai1	Hs00195591_m1
Snai2	Hs00161904_m1
Twist1	Hs00361186_m1
Vim	Hs00185584_m1
18S	Hs99999901_s1

Snai1, Snail family transcriptional repressor 1; Snai2, Snail family transcriptional repressor 2; Twist1, twist-related protein 1; Vim, vimentin.

https://erc.bioscientifica.com
https://doi.org/10.1530/ERC-23-0167

Transwell migration assay

Transwell migration assay was performed using 8 µm pore size transwell inserts (Greiner Bio-one, Kremsmünster, Austria). Briefly, tumour cells were seeds in complete RPMI at the density of 3×10^4 per insert and allowed to adhere overnight. The next day, the medium in the inserts was replaced with serum-free RPMI plus or not 30 nM or 1 µM of glibenclamide, while in the lower wells, complete RPMI was used as chemoattractant. After 16 h at 37°C, adherent cells in the upper part of the insert were removed, while cells migrated to the lower side of the inserts were fixed with cold methanol for 10 min, stained with 0.1% crystal violet and observed under the microscope. Images were acquired using a light microscope. To obtain a quantitative analysis, stained cells were eluted with DMSO, and the crystal violet released in the solution was quantified as OD at 560 nm by the spectrophotometer VICTOR^3 1420 Multilabel Counter (Packard Instruments, Perkin-Elmer). Migration was normalized on total cell number (duplicates of cells migrated and not, for each cell line, were counted: $3.2 \times 10^4 \pm 0.01$ parental and $3.1 \times 10^4 \pm 0.01$ SDHB-deficient cells).

Electrophysiological records

For electrophysiological records, parental and SDHB-deficient hPheo1 cells were plated at low density (2×10^4 cells per well) in standard polystyrene-treated culture dishes (35 mm × 10 mm, Corning Incorporated, Corning, NY). The electrophysiological properties of the cells were evaluated at room temperature by the whole-cell patch-clamp technique as reported (Di Franco *et al.* 2016) under a Nikon Eclipse TE200 inverted microscope. Patch pipettes were obtained from borosilicate glass capillaries (GC150-7.5, Harvard apparatus LTD, Cambridge, MA, USA) by a two-stage vertical puller (Narishige, Amityville, NY, USA) to get a final tip resistance of 1.5-3 MΩ when filled with the internal solution. The pipette solution contained 130 mM KCl, 10 mM NaH_2PO_4, 0.2 mM $CaCl_2$, 1 mM EGTA, 5 mM MgATP and 10 mM HEPES. The pH was set to 7.2 with TEA-OH. For SDHB-deficient cells, Mg-free solution (107 mM KCl, 1 mM K_2SO_4, 10 mM EGTA and 10 mM HEPES) was used (Proks *et al.* 2010). ATP (1–5 mM) was delivered intracellularly through the patch pipette and added as potassium salt to avoid K_{ATP} channel activation (pH maintained at 7.2 with KOH) and the K_{ATP} blocker glibenclamide was used at 20 µM. The patch electrode contained a chloride ion-coated silver wire and was held on a CV203BU head-stage (Axon Instruments, Foster City, CA, USA) connected to a three-way coarse manipulator and micro-manipulator (Narishige, Amityville, NY, USA) as well as to the Axopatch 200 B amplifier (Axon Instruments, Foster City, CA, USA). During recordings, cells were superfused at the rate of 1.8 mL/min with a physiological solution comprising 150 mM NaCl, 5 mM KCl, 2.5 mM $CaCl_2$, 1 mM $MgCl_2$, 10 mM D-glucose and 10 mM HEPES. The pH was set to 7.4 with NaOH. Pulse protocol generation and data acquisition were achieved by the A/D-D/A interfaces (Digidata 1200; Axon Instruments, Foster City, CA, USA) and Pclamp 6 software (Axon Instruments, Foster City, CA, USA). The RMP was measured in the current clamp mode of the 200 B amplifier using the current stimulus $I = 0$ nA. The membrane's passive properties were evoked in voltage-clamp mode applying a voltage pulse of ±10 mV starting from a holding potential (HP) of −70 mV, as reported (Di Franco *et al.* 2016, Squecco *et al.* 2020). The resulting current responses were analysed by the Clampfit 9 software (Axon Instruments, Foster City, CA, USA). In particular, the decay of the recorded passive current was fitted by an exponential function and the linear membrane capacitance (Cm) was calculated from the area under the capacitive transient current. The Cm value is used as an index of the cell surface area since the membrane-specific capacitance is assumed to be 1 µF/cm^2. Membrane resistance (Rm) was calculated from the steady-state membrane current (Im) as described (Squecco *et al.* 2020). Ion currents were evoked from HP = −80 mV by applying step voltage pulses, 1 s long, from −80 to 50 mV, in 10 mV increments. Current–voltage relationships were estimated by measuring the steady-state current obtained in response to the applied voltage steps with on-line leak subtraction ($P/4$). The currents were low-pass filtered with a Bessel filter at 2 KHz. To compare properly the current amplitudes elicited in cells of different dimensions, we normalized their values to Cm. Thus, the ratio I/Cm is considered as current density.

Statistical analysis

Data analyses were performed by the computer program GraphPad Prism Version 8.3.0 for Windows (GraphPad Software). Metabolic and functional experiments were conducted at least three times independently, with three or four replicates for each experimental condition. Electrophysiological data were obtained from randomly

https://erc.bioscientifica.com
https://doi.org/10.1530/ERC-23-0167

chosen portions of total cell populations. Results are expressed as mean ± S.D. The Student's *t*-test was used to compare the means between two sets of data. One-way analysis of variance followed by Bonferroni's *post hoc* test was used for multiple comparisons.

Results

Depletion of *SDHB* impairs cell metabolism

The efficiency of knocking out the SDHB subunit in hPheo1 cells was confirmed by Western blotting, which showed very low levels of the SDHB protein, while it did not affect the levels of other subunits such as SDHA or SDHD (Fig. 1A). In SDHB-deficient cells, we also observed a functional impairment of SDH enzyme activity that was significantly reduced by approximately 50%, compared to parental cells (Fig. 1B).

Moreover, the alteration of SDH function was also demonstrated by a considerable increase in the intracellular succinate/fumarate ratio, coupled with a decrease in the intracellular ATP concentration in SDHB-deficient cells compared to parental cells (Fig. 1C and D, respectively). We also observed a significant accumulation of intracellular lactate in SDHB-deficient cells (Fig. 1E), further supporting a marked metabolic shift from oxidative phosphorylation to aerobic glycolysis. This was linked to a significant decrease of pH (6.998 ± 0.04 vs 7.23 ± 05) and to a significant increase of lactate (9.7 ± 0.09 vs 5.3 ± 0.15) in culture media of SDHB-deficient cells compared to that of parental (Fig. 1F and G, respectively). Accordingly, we found

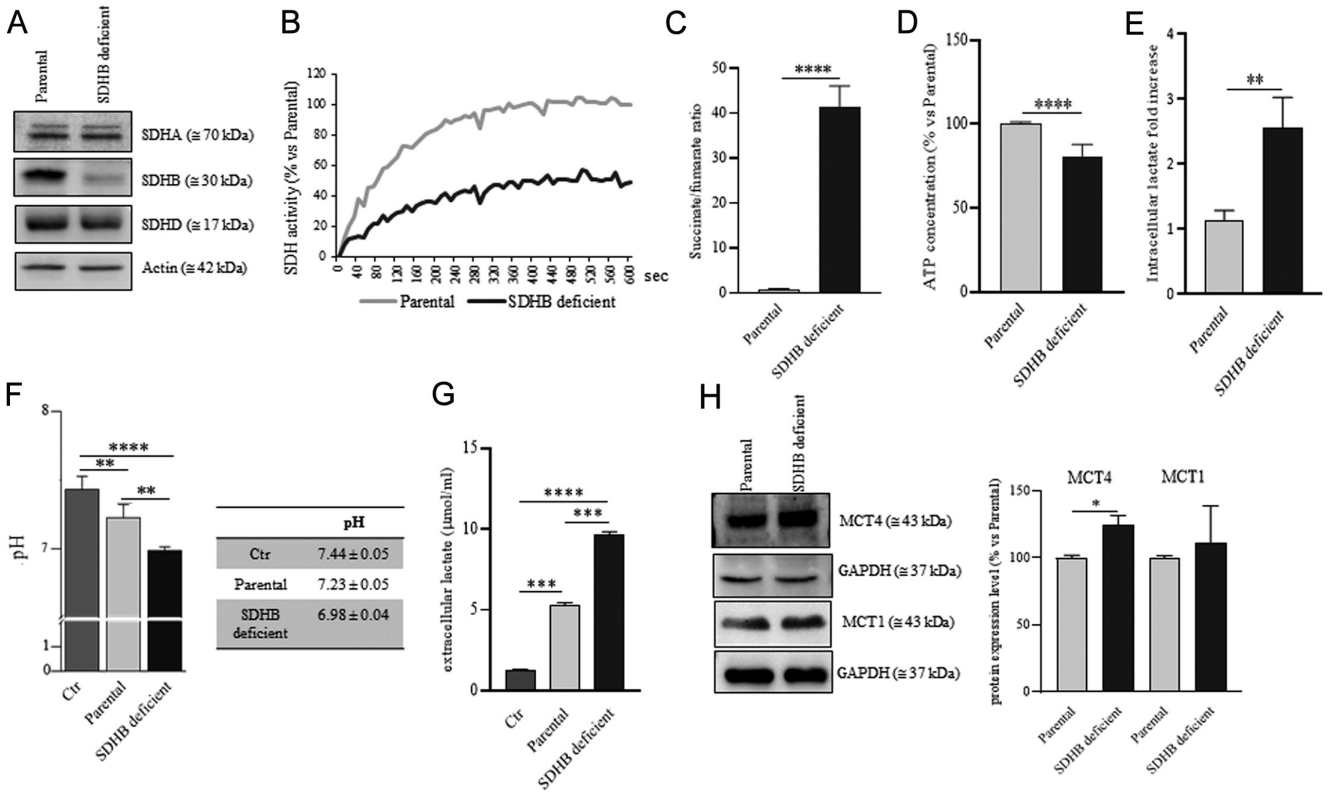

Figure 1
Effects of SDHB depletion on cell metabolism. (A) Representative blots showed the levels of SDHA, SDHB and SDHD subunits. Actin was used as loading control. (B) Representative traces of SDH enzymatic activity measured in parental and SDHB-deficient homogenates. The SDHB-deficient cells (dark grey line) showed a decrease in SDH activity of approximately 60% compared with parental (light grey line). (C) The bar graph shows the significant increase of the intracellular succinate/fumarate ratio, assessed by GC/MS, in SDHB-deficient cells compared with parental. (D) Intracellular ATP concentration in SDHB-deficient cells was significantly reduced compared to parental cells. (E) A significant increase in intracellular lactate levels, measured by GC/MS, was observed in SDHB-deficient cells. (F) pH measurement showed acidification of the media of both parental and SDHB-deficient cells, but the pH of SDHB-deficient cell media was significantly lower than that of parental cells. (G) Extracellular lactate concentration was significantly higher in SDHB-deficient cells compared to parental ones. (H) Representative blots and densitometric evaluation of MCT4 expression, which was significantly upregulated in SDHB-deficient cells vs parental ones, and MCT1 expression, which was unchanged between the two cell populations. GAPDH was used as loading control. Bar graphs are derived from three or four independent experiment, each of them conducted in triplicate, ± S.D. (*$P < 0.05$, **$P < 0.01$, ***$P < 0.001$, ****$P < 0.0001$.)

https://erc.bioscientifica.com
https://doi.org/10.1530/ERC-23-0167

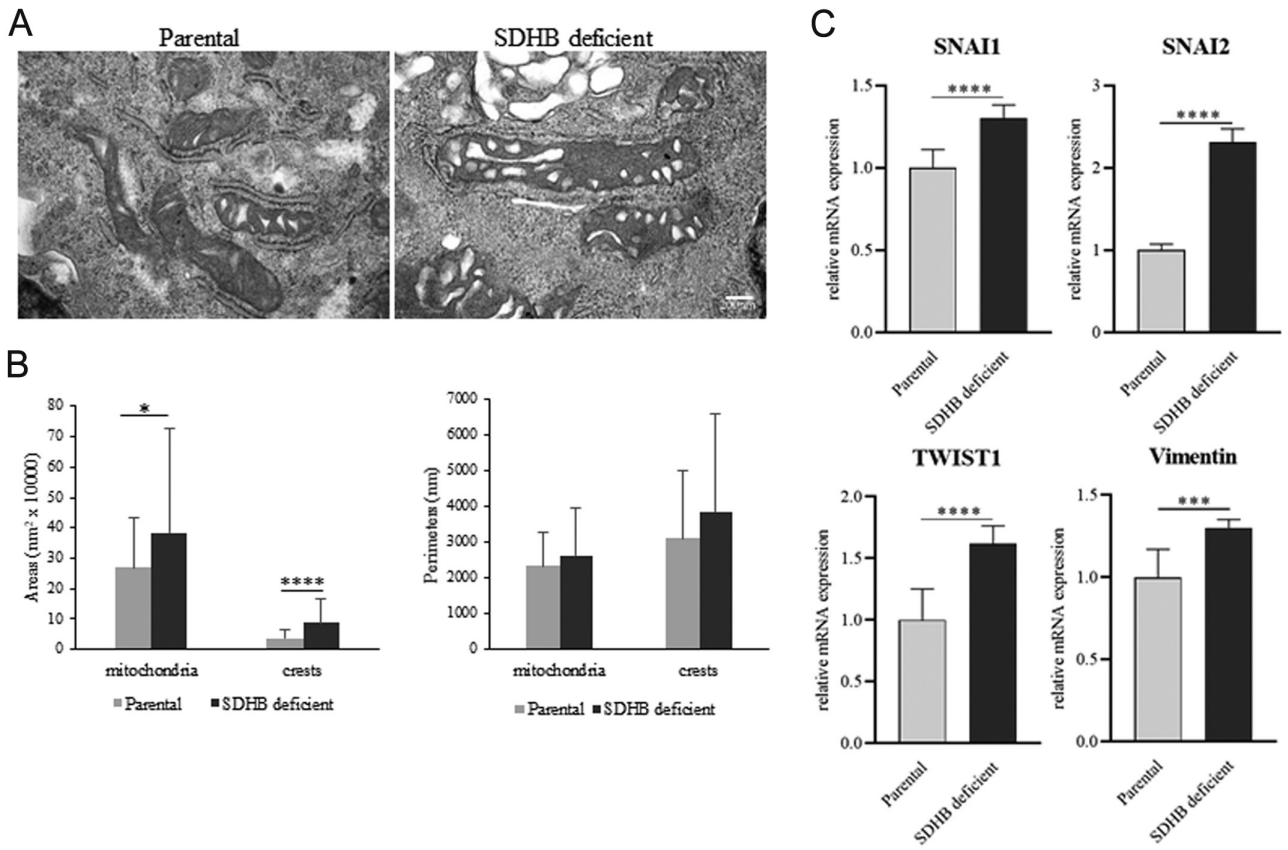

Figure 2
Characterization of mitochondrial morphology and EMT process. (A) Ultrathin sections of parental and SDHB-deficient cell were examined under a JEM 1010 electron microscope. Micrographs were taken using a Veleta Radius digital camera (EMSIS, Muenster, Germany). In SDHB-deficient cells, mitochondrial cristae appear slightly less compact than in parental cells. Scale bar = 200 nm. (B) The bars graph showed the areas and perimeters of mitochondria and mitochondrial cristae in parental ($n = 44$) and SDHB-deficient cells ($n = 33$). In SDHB-deficient cells, the areas of both mitochondria and mitochondrial cristae were significantly increased compared to parental ones. On the other hands, no significant differences were observed in mitochondria and cristae perimeters. The analysis was obtained using iTem Soft Imaging System program. (C) qRT-PCR analysis demonstrated a significant upregulation of Snai1, Snai2, Twist1 and Vimentin in SDHB-deficient cells compared to the parental ones. (*$P < 0.05$, ***$P < 0.001$, ****$P < 0.0001$.)

increased expression of the MCT4, while MCT1 expression was not affected (Fig. 1G).

SDHB-deficient cells display mitochondrial cristae disorganization and epithelial–mesenchymal transition (EMT)-like phenotype

Electron microscopy analysis revealed less compact mitochondrial cristae in SDHB-deficient cells compared to parental ones (Fig. 2A). This observation was demonstrated by the computational analysis of mitochondria and mitochondrial cristae areas and perimeters in our cells (Fig. 2B). SDHB-deficient cells showed both mitochondria and cristae areas higher than those of the parental ones, but interestingly, perimeters did not differ between the two cell populations, confirming that in SDHB-deficient cells, mitochondria were swollen and cristae were less compact.

Recently, Tabebi and colleagues (Tabebi *et al.* 2022) found that several genes involved in EMT were upregulated in hPheo1 SDHB-deficient cells compared with controls. By qRT-PCR, we confirmed that the expression of the main markers of EMT, such as *Twist1*, *Snai1*, *Snai2* and *Vimentin*, was significantly increased in SDHB-deficient cells (Fig. 2C), suggesting that these cells undergo a transcriptional reprogramming associated with an EMT phenotype.

Membrane electrical features and K^+ currents in SDHB-deficient cells: effects of glibenclamide and ATP

Unlike other pheochromocytoma cell lines, such as the mouse pheochromocytoma cell (MPC) line and the mouse tumour tissue-derived cell (MTT) line, hPheo1 cells do not grow in clusters, allowing us to analyse the electrophysiological properties of single cells by the

https://erc.bioscientifica.com
https://doi.org/10.1530/ERC-23-0167

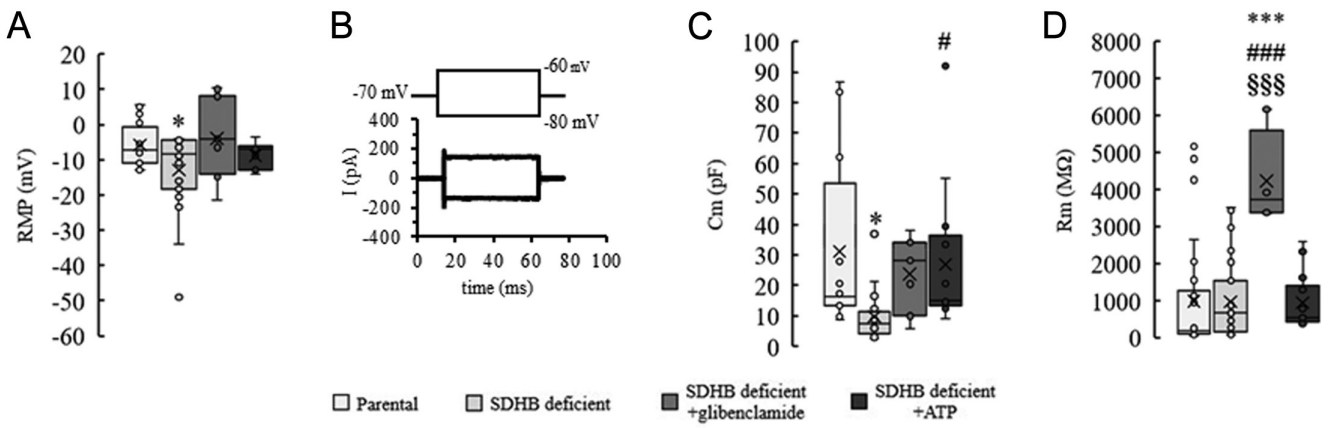

Figure 3

Analysis of parental and SDHB-deficient cell membrane passive properties. Data related to all of the conditions have been here plotted together to better highlight differences and similarities. (A) Resting membrane potential, RMP (in mV), evaluated in current-clamp mode with $I = 0$ nA in parental cells ($n = 20$), SDHB-deficient cells ($n = 23$), SDHB-deficient cells + glibenclamide ($n = 11$) and SDHB-deficient cells after intracellular delivery of ATP by the patch pipette ($n = 11$). SDHB-deficient cells showed significantly more hyperpolarized RMP compared to parental cells, but in the presence of glibenclamide and ATP, RMP was restored. (B) Voltage pulse protocol of stimulation (upper panel) and typical passive currents (lower panel) obtained in response to its application under voltage clamp condition. (C) Cell capacitance, Cm (in pF), estimated in voltage-clamp mode in parental cells ($n = 12$), SDHB-deficient cells ($n = 17$), SDHB-deficient cells + glibenclamide ($n = 7$) and SDHB-deficient cells after intracellular delivery of ATP by the patch pipette ($n = 13$). Cm is significantly smaller in SDHB-deficient cells compared to parental cells. Cm significantly increased after ATP delivery in SDHB-deficient cells compared to SDHB-deficient ones. Cm of SDHB-deficient cells + glibenclamide or + ATP and parental ones were not significantly different. (D) Membrane resistance, Rm, values (in MΩ) measured in parental cells ($n = 37$), SDHB-deficient cells ($n = 35$), SDHB-deficient cells + glibenclamide ($n = 8$) and SDHB-deficient cells after intracellular delivery of ATP by the patch pipette ($n = 20$). Rm values obtained in the presence of glibenclamide resulted significantly bigger compared to any other condition. Data are mean values ± S.D. ($^{*}P < 0.05$, $^{***}P < 0.001$ vs parental; $^{\#}P < 0.05$, $^{\#\#\#}P < 0.001$ vs SDHB deficient; $^{\S}P < 0.05$; $^{\S\S\S}P < 0.001$ vs SDHB deficient + ATP. One-way ANOVA, with Bonferroni's correction).

whole cell patch-clamp technique. We first measured the RMP values of the two cell populations in the current clamp mode. SDHB-deficient cells resulted in being significantly more polarized (−11.9 ± 11.7 mV; $n = 23$) than parental cells (−5.8 ± 6.1 mV; $n = 20$) (Fig. 3A). We then analysed the cell passive properties that represent membrane electrical features allowing excitable cells to conduct electrical impulses without involving voltage-dependent ion channels. They determine the membrane potential changes in response to current across the cell membrane (linearly with a current stimulus application). They are mainly represented by Rm and Cm that herein were estimated from current traces evoked by suitable step voltage pulses, sufficiently negative to avoid the appearance of voltage-dependent currents. The pulse protocol of stimulation and the typical current responses are depicted in Fig. 3B. The calculated Cm values, used as an index of cell surface area, were found to be significantly smaller in SDHB-deficient than in parental cells, being 10.2 ± 8.5 pF ($n = 17$) and 31.6 ± 28.9 pF ($n = 12$), respectively (Fig. 3C). Rm values in SDHB-deficient (647.05 ± 700.1 MΩ; $n = 30$) did not show statistically significant differences compared to parental cells (982.03 ± 1449.1 MΩ, $n = 37$), suggesting a scarce effect of this condition on membrane-resting permeability (Fig. 3D).

Analysis of ion currents under voltage clamp condition (pulse protocol depicted in Fig. 4A) recorded from parental cells revealed the occurrence of outward K^+ currents with the time course and *I–V* relation typical of voltage-dependent currents (Rhie *et al.* 1999), with a voltage activation threshold of about −10 mV (Fig. 4B and F, respectively). In contrast, analysis of SDHB-deficient cells revealed a larger mean current amplitude and a lack of voltage threshold significantly different to parental cells, as shown in Fig. 4C and F, respectively. Notably, this greater outward current agrees with the observed resting membrane potential that is more hyperpolarized in SDHB-deficient cells than in parental cells. Since the related *I–V* plot brought to mind that reported for ATP-sensitive K^+ currents (Shi *et al.* 2019), and since these cells showed reduced intracellular ATP content because of SDHB deficiency, to test the occurrence of possible K_{ATP} currents, we performed two different sets of experiments. In the first, we used the specific K_{ATP} channels inhibitor, glibenclamide (Shi *et al.* 2019). In the second, to overcome the effect of low intracellular concentration of ATP on K_{ATP} channels, we carried out experiments in which intracellular ATP content was raised by adding the nucleotide in the form of a K^+ salt (Proks *et al.* 2010). Interestingly, both glibenclamide and

https://erc.bioscientifica.com
https://doi.org/10.1530/ERC-23-0167

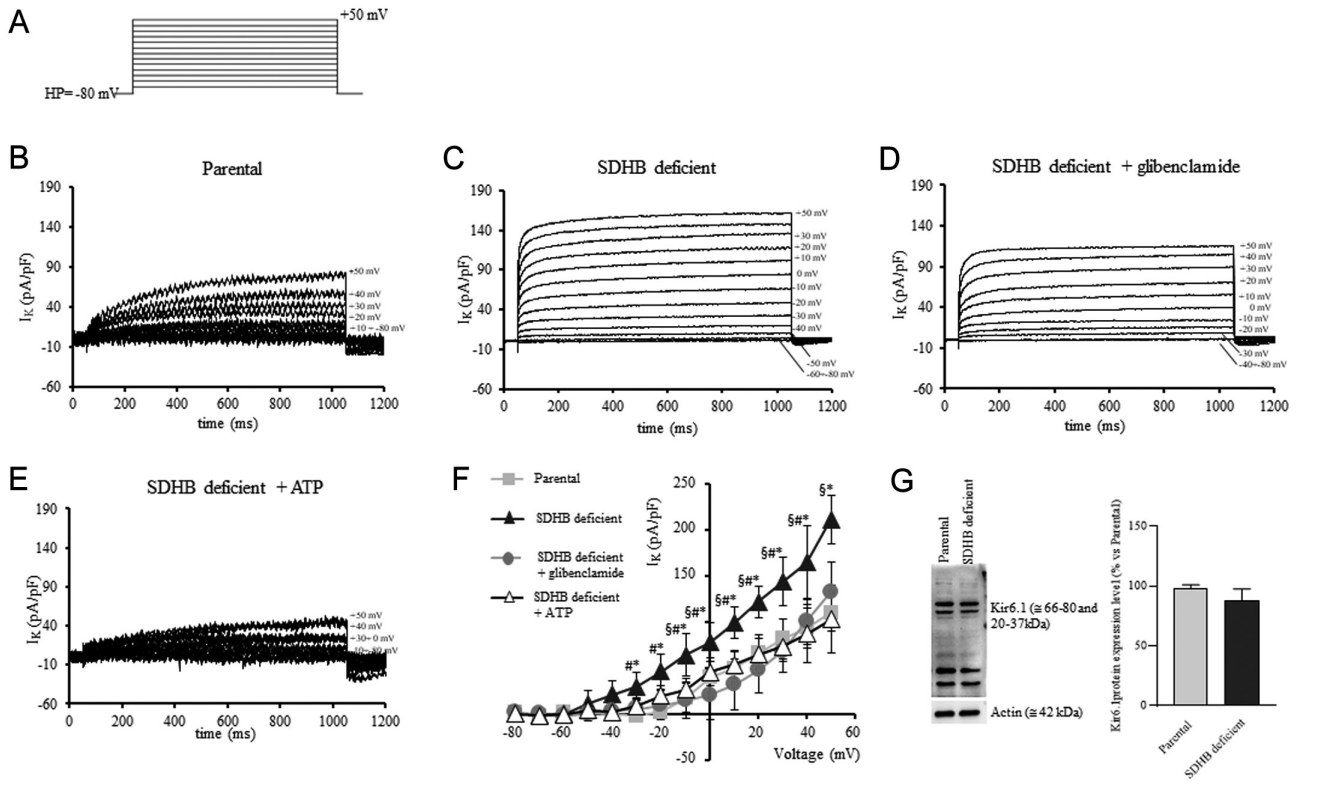

Figure 4

Analysis of K⁺ currents in parental and SDHB-deficient cells: effects of glibenclamide and ATP. (A) Voltage pulse protocol of stimulation (HP = −80 mV) used to evoke the current responses. Representative traces of normalized outward K⁺ currents (pA/pF) elicited in a parental (B) and in a SDHB-deficient cell (C). (D) Typical records obtained in the presence of the selective K_{ATP} blocker glibenclamide (20 μM) in the same SDHB-deficient cell as reported in B. (E) Representative traces of normalized outward K⁺ currents (pA/pF) evoked in an SDHB-deficient cell after intracellular delivery ATP by the patch pipette. (B–E) The voltage step pulse evoking each current response is indicated in mV next to the corresponding trace. When current responses are superimposed, this indication is given as a voltage range for clarity. (F) *I–V* curves related to I_K in parental ($n = 4$), in SDHB-deficient cells in the absence ($n = 4$) and in the presence of glibenclamide 20 μM ($n = 4$) and in ATP-rescued SDHB-deficient cells ($n = 4$), here plotted together to better highlight differences and similarity. Data from SDHB-deficient cells are significantly different from those obtained in parental cells starting from voltages more depolarized than −30 mV (*$P < 0.05$). Results from SDHB-deficient cells + glibenclamide and from ATP-rescued SDHB-deficient cells are not significantly different neither between them ($P > 0.05$) nor compared to parental cells ($P > 0.05$) for any voltage step applied. In contrast, statistically significant differences were observed for SDHB-deficient cells + glibenclamide vs SDHB-deficient cells starting from −30 mV up to +50 mV (#$P < 0.05$) and for ATP-rescued SDHB-deficient cells vs SDHB-deficient cells for any voltage step positive to −10 mV (§$P < 0.05$). Data are mean values ± S.D. One-way ANOVA, with Bonferroni's correction. (G) Representative blots (left) and densitometric evaluation (right) of Kir6.1 expression level, which did not differ between parental and SDHB-deficient cells. Actin was used as a loading control.

ATP caused a significant reduction in outward currents compared to those recorded from SDHB-deficient cells (Fig. 4D, E and F, with a statistical significance at voltage steps from −30 up to +50 mV and for any voltage step positive to −10 mV, respectively). Moreover, the outward currents recorded in the presence of glibenclamide or ATP resulted not significantly different from those of the parental cells. Noteworthy, glibenclamide also restored the voltage threshold of appearance at −10 mV, as observed in parental cells (Fig. 4F). These results indicate the presence of the K_{ATP} current in the overall currents recorded in these cells. We also evaluated whether the difference in K⁺ currents might have been associated with a different expression of the K_{ATP} channel Kir6.1, but as shown in Fig. 4G, Kir6.1 was not differentially expressed in the two cell populations.

A similar outcome was observed for passive properties when glibenclamide or ATP was added to the bath solution. In fact, when compared to those measured from untreated SDHB-deficient cells, the RMP values tended to be more depolarized after glibenclamide addition, being −4.02 ± 10.4 mV ($n = 11$; Fig. 3A), Cm values increased to 24.22 ± 12.2 pF ($n = 7$, Fig. 3C) and, as expected, following the use of a channel blocker, Rm significantly increased to 4235.1 ± 1215.8 MΩ ($n = 8$) (Fig. 3D). In ATP-rescued SDHB-deficient cells, RMP value increased to −8.8 ± 3.5 mV ($n = 11$, Fig. 3A), Cm increased to 27.32 ± 23.7 ($n = 13$, Fig. 3C) and Rm

https://erc.bioscientifica.com
https://doi.org/10.1530/ERC-23-0167

increased to 936.7 ± 733.9 MΩ (n = 20) (Fig. 3D) compared to those recorded from untreated SDHB-deficient cells. Again, after both treatments, the passive properties of the SDHB-deficient cells were no longer statistically different from those of parental cells, suggesting a partial recovery of biophysical properties induced by blocking K_{ATP} channels. Overall, these data indicate that one of the main differences between SDHB-deficient and parental cells' bioelectric profiles is due to K_{ATP} channel engagement in the former population.

Functional characteristics of SDHB-deficient cells are related to their bioelectrical features

We next investigated whether parental and SDHB-deficient cells showed differences in their functional characteristics and whether, by restoring the electrophysiological properties of SDHB-deficient cells by glibenclamide, the differences in functional features could also be eventually re-established. First of all, when we analysed cell growth, we found that

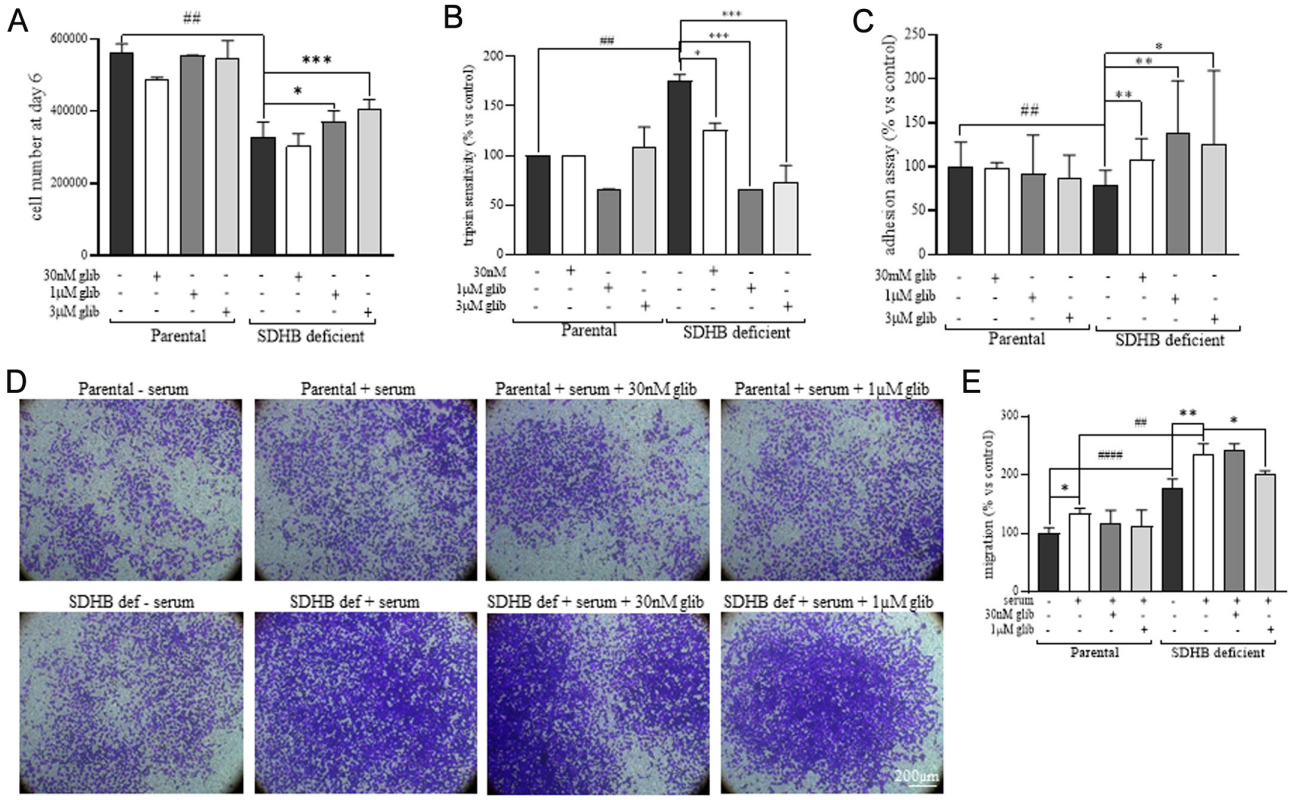

Figure 5

Analysis of functional properties and role of glibenclamide in their modulation. (A) Cell number at day 6 in the absence (black bars) or in the presence of 30 nM (white bars), 1 μM (dark grey bars) and 3 μM (light grey bars) of glibenclamide (abbreviation: Glib). SDHB-deficient cells significantly increased their growth capacity after 1 μM and 3 μM of glibenclamide treatment. The administration of 30 nM of glibenclamide did not affect the proliferation of both cell populations. (B) SDHB-deficient cells displayed higher sensitivity to trypsin treatment compared to parental cells. This sensitivity was significantly reduced by glibenclamide at all doses. (C) Adhesion capacity was assessed using the Bengal rose assay. SDHB-deficient cells showed a significantly less efficient adhesion capability compared to parental cells. All doses of glibenclamide tested caused a significant increase in SDHB-deficient adhesion capacity. (D) Parental and SDHB-deficient cell migration through 8 μm porous transwell membranes in the presence or absence of serum with or without 30 nM or 1 μM of glibenclamide for 16 h. Images are representative of migrating cells of three independent experiments, each performed in duplicate. Scale bar = 200 μm. Migration was normalized on total cell number (migrated and not), and no differences was observed in SDHB-deficient and parental cell number ($3.2 \times 10^4 \pm 0.01$ and $3.1 \times 10^4 \pm 0.01$, respectively). (E) Quantification of parental and SDHB-deficient cell migration reported as percentages. In the presence (white bars) or in the absence (dark grey bars) of serum, SDHB-deficient cells migrated significantly more compared with parental cells. Addition of 30 nM of glibenclamide did not affect either parental either SDHB-deficient cell migration (dark grey bars). In contrast, treatment with 1 μM of glibenclamide (light grey bars) induced a significant reduction of migration only in SDHB-deficient cells. All data are the mean values of three independent experiments, each conducted in triplicates, ± S.D. Hashtags indicate the statistic of values between parental and SDHB deficient ($^{\#\#}P < 0.01$, $^{\#\#\#\#}P < 0.0001$), while asterisks indicate the statistical differences between parental or SDHB-deficient treated or not glibenclamide ($^{*}P < 0.05$, $^{**}P < 0.01$, $^{***}P < 0.001$).

https://erc.bioscientifica.com
https://doi.org/10.1530/ERC-23-0167

SDHB-deficient cells had a reduced proliferation rate compared to parental cells (Fig. 5A). Interestingly, we observed that the number of SDHB-deficient cells was significantly increased after 6 days of glibenclamide (1 and 3 µM) treatment compared to the untreated counterpart. In contrast, the treatment with the same doses of the K_{ATP} channel inhibitor on parental cells did not have the same effect. The treatment with glibenclamide 30 nM did not influence either parental or SDHB-deficient cell proliferation (for all the doses tested see Supplementary Fig. 1, see section on supplementary materials given at the end of this article). We next tested whether SDHB-deficient and parental cells were sensitive to detachment after trypsinization for 1 min. This test is used to distinguish differentially adherent cell types (Morata-Tarifa *et al.* 2016). We found that the number of SDHB-deficient cells detached after trypsin treatment was significantly higher compared to parental cells. Interestingly, glibenclamide treatment, at all the doses tested, was able to reduce the number of SDHB-deficient cells detached (Fig. 5B). In another experiment, we investigated the adhesion potential of both parental and SDHB-deficient cells in the presence or not of glibenclamide. After 4 h of plating, non-adherent cells were removed while adherent ones have been quantified using Bengal rose staining. By this assay, we showed that SDHB-deficient cells had a significantly lower adhesion capacity compared to parental cells (Fig. 5C), but glibenclamide addition induced a significant increase in adhesion in these cells. In contrast, glibenclamide did not cause appreciable effects in parental cells. To further explore the migration abilities of the two cell lines, we used the transwell assay technique, in which we stained the migrated cells (Fig. 5D) and quantified the eluted dye by optical density (Fig. 5E). We found that SDHB-deficient cells showed a significantly higher migration ability compared to parental cells, regardless the absence or presence of the chemoattractant, represented by the serum, in the lower wells. Moreover, we observed a significant reduction of SDHB-deficient cell migration only after the administration of 1 µM glibenclamide for 16 h. On the contrary, glibenclamide did not have any effects on parental cell migration.

Discussion

In the present study, we provide evidence that the loss of SDHB subunit affects electrophysiological features of human pheochromocytoma cells, which in turn leads to functional changes that can be related to an increase in their aggressiveness. Importantly, we also demonstrate for the first time that, *in vitro*, the enhanced migratory ability of SDHB-deficient cells was significantly inhibited by restoring their bioelectrical properties following glibenclamide treatment.

It is known that transmembrane ion fluxes not only contribute to cell excitability but also play a noteworthy role in proliferation, cell cycle progression, and cell maturation and differentiation. Ion flows determine, for instance, the RMP, the voltage across the resting plasma membrane established by the balance of extracellular and intracellular ion concentrations. Such a balance is regulated by the activity of different ion channels, pumps and transporters located within the cell membrane that have specific ion selectivity and permeability. RMP is considered a fundamental regulator of cell behaviour in both excitable and non-excitable cells, modulating important cell functions such as proliferation and differentiation (Sundelacruz *et al.* 2009). Thus, bioelectric properties can be useful markers for cell characterization because they are related to cell cycle progression, cell mitotic activity and differentiation. Interestingly, electrophysiological studies in several cancer cell types (Yang & Brackenbury 2013) have revealed depolarized membrane potential that favours cell proliferation: cancerous cells tend to have a depolarized RMP and are mitotically highly active. In contrast, more quiescent cells show more hyperpolarized membrane and show low mitotic activity (Sundelacruz *et al.* 2009). In line with this observation, our results have actually documented that SDHB-deficient cells, which have a more negative membrane potential, exhibit a lower proliferative status compared to parental cells.

Another interesting finding is related to the analysis of passive properties. In particular, Cm, the electrical capacitance of cell membrane, is strictly connected to the membrane composition consisting of phospholipid bilayer with which various proteins are 'associated'. Therefore, the overall Cm of a cell is a value directly proportional to the membrane surface area and the dielectric properties of the membrane. For this reason, Cm is usually considered an index related to the cell surface. A thorough evaluation of this parameter could be used as an alternative marker for assessing cell proliferation for a wide field of applications, including cancer research. In this regard, Prakash and Abshire (Prakash & Abshire 2008) employed integrated capacitance sensors for monitoring the growth of

https://erc.bioscientifica.com
https://doi.org/10.1530/ERC-23-0167

anchorage-dependent cells from breast cancer and observed an increased Cm value in response to cell adhesion that is usually followed by elevated proliferation. According to these observations, our experimental results revealed significantly lower Cm values in SDHB-deficient cells compared to parental, which were indeed less adherent and featured lower proliferation.

Interestingly, analysis of the ion currents in parental cells revealed the occurrence of outward K^+ currents and an *I–V* relation typical of voltage-dependent currents (Rhie *et al.* 1999). In contrast, analysis of SDHB-deficient cells showed that they feature greater mean amplitude and lack of voltage threshold. Of note, this larger outward current agrees with the significantly more hyperpolarized RMP observed in SDHB-deficient cells compared to parental cells. The voltage dependence of this current, estimated by the *I–V* plot analysis, resembled that reported for currents flowing through ATP-sensitive potassium channels (K_{ATP}) (Shi *et al.* 2019), which are considered electrical transducers of the metabolic state of a cell by coupling cellular metabolism to the membrane potential (Nichols 2006). Since SDHB-deficient cells showed reduced intracellular ATP content due to impaired SDH activity that is expected to trigger K_{ATP} channel activation, we performed experiments using the K_{ATP} channel inhibitor glibenclamide (Shi *et al.* 2019). We indeed observed that glibenclamide significantly reduced the outward current, indicating a substantial implication of K_{ATP} current in the overall outward current. Noteworthy, the ion current recorded in the presence of glibenclamide, when K_{ATP} channels are blocked, showed a voltage threshold not statistically different to that seen in parental cells, suggesting that K_{ATP} channels are primarily activated in SDHB-deficient cells. Moreover, glibenclamide addition to SDHB-deficient cells determined a substantial recovery also of the passive properties showing similar values to those observed in parental cells. As expected, the Rm value following the use of the channel blocker was definitely increased. In fact, channel blockers normally reduce the membrane conductance since they inhibit ion fluxes through those channels open in the resting cell that contribute to keep the membrane resistance low (Ostroumov *et al.* 2011).

Although K_{ATP} channels are expressed on the cell surface membranes, several studies reported their presence also on mitochondria (Busija *et al.* 2004, Zhao *et al.* 2021). This may not be surprising, since mitochondria are the major producers of ATP and the main users of O_2, K_{ATP} channels are strategically located to sense changes in metabolite amount (Pamenter 2014, Country & Jonz 2021, Maqoud *et al.* 2022). However, despite the possible presence of K_{ATP} channels on the mitochondrial membrane (mK_{ATP} channels) in our cell model, the whole cell patch clamp technique applied in our study likely consents us to record phenomena occurring on the plasma lemma or, eventually, on membrane systems in continuity with it, not comprising events occurring on internal organelles. Based on this observation, we may reasonably suppose that glibenclamide effects observed on electrophysiological records are those on plasma membrane K_{ATP} channels. It is unclear if glibenclamide addition might affect mK_{ATP}, but even if it could do it, this effect may not be observable in our current recordings. In this regard, Country and Jonz, by the whole-cell patch-clamp recordings, found that plasma membrane currents were not influenced by mK_{ATP} channel drugs in isolated goldfish retinal horizontal cells (Country & Jonz 2021).

Further evidences for a role of K_{ATP} channels in SDHB-deficient cells' behaviour comes from experiments in which the addition of ATP, which is expected to have an inhibitory effect on K_{ATP} channels, also caused passive properties normalization of SDHB-deficient cells. At the same time, the outward current time course and the *I–V* plot related to experiments carried out under this condition indeed resembled the pattern of parental cells, showing not statistically significant differences compared to them. This indicates that SDHB-deficient cells feature K^+ channel activation similar to their parental counterparts when the ATP content is restored, underlining the role of the metabolic condition in determining peculiar bioelectrical properties. Interestingly, since our results showed no differences in Kir6.1 expression, it is reasonable to conclude that the differences observed in electrophysiological recordings of outward K^+ currents are related only to different functional activation of K_{ATP} channels and not to changes in theirexpression levels.

It is known that tumour cells show a shift from oxidative phosphorylation to aerobic glycolysis even in the presence of oxygen, a phenomenon known as Warburg effect (Warburg *et al.* 1927). In addition to the lower ATP concentrations, SDHB-deficient cells showed increased intracellular lactate production followed by a reduced culture media pH compared with parental cells. These results could be explained by the fact that cancer cells, typified by higher expression of regulators such as monocarboxylate transporters (MCTs), can

https://erc.bioscientifica.com
https://doi.org/10.1530/ERC-23-0167

mobilize lactic acid to the extracellular environment, whereby maintaining the intracellular pH homeostasis while decreasing the extracellular pH, as found for SDHB-deficient cells. Furthermore, SDHB-deficient cells showed a lower proliferation rate compared to parental cells. These results are in line with our data previously obtained on MTT cells silenced for SDHB (Richter *et al.* 2018), where we observed a lower proliferation rate. The association between deletion of SDHB and low proliferation has been demonstrated also for breast cancer (Bezawork-Geleta *et al.* 2016).

From an ultrastructural point of view, using electron microscopy, we showed that *SDHB* depletion resulted in enlarged mitochondria and poorly organized internal cristae. This observation is consistent, albeit to a lesser extent, with the earlier report by Douwes Dekker and colleagues that *SDHD*-linked tumours have swollen mitochondria with loss of cristae (Douwes Dekker *et al.* 2003).

Loriot and colleagues observed that EMT was activated in human metastatic SDHB-mutated PPGLs (Loriot *et al.* 2012). Few years later, the same research group showed that in SDHB knockout mouse chromaffin cells occurred a molecular reprogramming compatible with the activation of EMT process (Loriot *et al.* 2015). More recently, Tabebi and colleagues (Tabebi *et al.* 2022) observed an upregulation of several genes involved in EMT in a SDHB knockout model of hPheo1. In accordance, we show that SDHB deficiency in hPheo1 cells leads to a transcriptional upregulation of *Twist1, Snai1/2* and *Vimentin*. Remarkably, Tabebi *et al.* also found a significant increase in the percentage of trypsin-sensitive cells due to SDHB loss, that is in agreement with our results. The association between trypsin sensitivity and migration is very limited; however, Zhu and colleagues (Zhu *et al.* 2018) described this correlation in three different cancer cell lines, the MB49, the EJ and the SKOV3. Depletion of *SDHB* altered adhesion properties of the extracellular matrix by increasing trypsin sensitivity, by decreasing adhesion capacity and by inducing the acquisition of an EMT phenotype, therefore promoting a more malignant profile (Walia & Elble 2010, Loriot *et al.* 2015, Pastushenko & Blanpain 2019).

In this work, we showed that SDHB-deficient cells proliferate less than parental cells but migrate significantly more, supporting their more aggressive phenotype. This result not only is consistent with what was found in SDHB knockout mouse chromaffin cells (Loriot *et al.* 2015) but also with our previous data obtained with another chromaffin cell model, the MTT cells. In fact, in this cell line, we observed a higher migratory trend in single cultured MTT SDHB-silenced spheroids compared with single cultured MTT Wt spheroids (D'Antongiovanni *et al.* 2017). Furthermore, when spheroids were co-cultured with cancer associated fibroblast (CAFs), despite we observed a massive migration induction, the number of the cells was smaller compared to their single cultured counterpart (Martinelli *et al.* 2022), supporting our hypothesis that the high motility is inversely related to cell proliferation and *vice versa*. Indeed, the addition of glibenclamide significantly promoted proliferation and adhesion but significantly reduced migration and trypsin sensitivity of these cells.

One of the strengths of this study is that hPheo1 cells and their SDHB-deficient counterparts (Ghayee *et al.* 2013, Matlac *et al.* 2021) are the only available human pheochromocytoma cells, which makes them a plausible candidate to increase our understanding of the fundamental mechanisms involved in oncogenesis and tumour development of PPGLs. The main feature of pheochromocytomas and sympathetic paragangliomas is the release of catecholamines such as epinephrine, norepinephrine or dopamine (Lenders *et al.* 2020). However, characterization of hPheo1 cells showed that even if genes associated with catecholamine synthesis were highly expressed in the tumour tissue of origin, most of them were downregulated in hPheo1 cells. Consequently, one of the limits of this work is linked to the impossibility of studying the currents involved in catecholamine secretion. Despite the lack of hormone production, we provide here novel insights into the role of SDH that, by altering the metabolic characteristics of human pheochromocytoma cells, modulates their bioelectric properties which, in turn, affect some functional features and increase their aggressiveness. However, these functional alterations can be restored to some extent when the bioelectrical ones are recovered. Bioelectric signalling in cancer and particularly in metastasis is a growing field of study, which has demonstrated the importance in many of the key mechanisms of metastasis (Payne *et al.* 2022).

It is worth noting that all data presented here support the hypothesis that glibenclamide may exert significant anti-tumour activity in PPGLs by inhibiting K_{ATP} channels (Gao *et al.* 2017). In this regard, early studies have reported that glibenclamide could actually inhibit progression in many other cancers such as bladder carcinoma (Wondergem *et al.* 1998), prostate (Abdul & Hoosein 2002) and liver (Malhi *et al.* 2000).

https://erc.bioscientifica.com
https://doi.org/10.1530/ERC-23-0167

Moreover, in recent years, it has been demonstrated that glibenclamide can suppress cell invasion and migration in a human ovarian clear cell carcinoma ES-2 cells by blocking K_{ATP} channels (Yasukagawa *et al.* 2012). Further experiments should be performed to support our data, especially *in vivo* studies and the use of selective drugs targeting K_{ATP} channels will be of interest.

Taken together, our results highlight the importance of focusing also on cancer cell electrophysiological profile in order to eventually provide new approaches to targeting metastatic disease.

Supplementary materials

This is linked to the online version of the paper at https://doi.org/10.1530/ERC-23-0167.

Declaration of interest

The authors declare no conflicts of interest.

Funding

This research was supported by Italian Association for Cancer Research (AIRC, under IG 2020-ID 24820 project to Mario Maggi) and by the Andrological Sciences Onlus to E R and R S J N was supported in part by Czech Science Foundation (grants 21-04607X and 22-07091S). Martinelli S, Canu L, Rapizzi E and Maggi M are members of the Florence Center of Excellence recognized by the European Network for the Study of Adrenal Tumours (ENS@T).

References

Abdul M & Hoosein N 2002 Expression and activity of potassium ion channels in human prostate cancer. *Cancer Letters* **186** 99–105. (https://doi.org/10.1016/s0304-3835(02)00348-8)

Abdul M, Santo A & Hoosein N 2003 Activity of potassium channel-blockers in breast cancer. *Anticancer Research* **23** 3347–3351.

Aydar E, Yeo S, Djamgoz M & Palmer C 2009 Abnormal expression, localization and interaction of canonical transient receptor potential ion channels in human breast cancer cell lines and tissues: a potential target for breast cancer diagnosis and therapy. *Cancer Cell International* **9** 23. (https://doi.org/10.1186/1475-2867-9-23)

Becchetti A 2011 Ion channels and transporters in cancer. 1. Ion channels and cell proliferation in cancer. *American Journal of Physiology. Cell Physiology* **301** C255–C265. (https://doi.org/10.1152/ajpcell.00047.2011)

Bezawork-Geleta A, Dong L, Rohlena J & Neuzil J 2016 The assembly factor SDHAF2 is dispensable for flavination of the catalytic subunit of mitochondrial Complex II in breast cancer cells. *Journal of Biological Chemistry* **291** 21414–21420. (https://doi.org/10.1074/jbc.C116.755017)

Blackiston DJ, McLaughlin KA & Levin M 2009 Bioelectric controls of cell proliferation: ion channels, membrane voltage and the cell cycle. *Cell Cycle* **8** 3527–3536. (https://doi.org/10.4161/cc.8.21.9888)

Buffet A, Burnichon N, Favier J & Gimenez-Roqueplo AP 2020 An overview of 20 years of genetic studies in pheochromocytoma and paraganglioma. *Best Practice and Research. Clinical Endocrinology and Metabolism* **34** 101416. (https://doi.org/10.1016/j.beem.2020.101416)

Busija DW, Lacza Z, Rajapakse N, Shimizu K, Kis B, Bari F, Domoki F & Horiguchi T 2004 Targeting mitochondrial ATP-sensitive potassium channels--a novel approach to neuroprotection. *Brain Research. Brain Research Reviews* **46** 282–294. (https://doi.org/10.1016/j.brainresrev.2004.06.011)

Country MW & Jonz MG 2021 Mitochondrial KATP channels stabilize intracellular Ca2+ during hypoxia in retinal horizontal cells of goldfish (Carassius auratus). *Journal of Experimental Biology* **224**. (https://doi.org/10.1242/jeb.242634)

D'Antongiovanni V, Martinelli S, Richter S, Canu L, Guasti D, Mello T, Romagnoli P, Pacak K, Eisenhofer G, Mannelli M, *et al.* 2017 The microenvironment induces collective migration in SDHB-silenced mouse pheochromocytoma spheroids. *Endocrine-Related Cancer* **24** 555–564. (https://doi.org/10.1530/ERC-17-0212)

Dariane C, Goncalves J, Timsit MO & Favier J 2021 An update on adult forms of hereditary pheochromocytomas and paragangliomas. *Current Opinion in Oncology* **33** 23–32. (https://doi.org/10.1097/CCO.0000000000000694)

Di Franco A, Guasti D, Squecco R, Mazzanti B, Rossi F, Idrizaj E, Gallego-Escuredo JM, Villarroya F, Bani D, Forti G, *et al.* 2016 Searching for classical brown fat in humans: development of a novel human fetal brown stem cell model. *Stem Cells* **34** 1679–1691. (https://doi.org/10.1002/stem.2336)

Douwes Dekker PB, Hogendoorn PC, Kuipers-Dijkshoorn N, Prins FA, van Duinen SG, Taschner PE, van der Mey AG & Cornelisse CJ 2003 SDHD mutations in head and neck paragangliomas result in destabilization of complex II in the mitochondrial respiratory chain with loss of enzymatic activity and abnormal mitochondrial morphology. *Journal of Pathology* **201** 480–486. (https://doi.org/10.1002/path.1461)

Dubois JM & Rouzaire-Dubois B 1993 Role of potassium channels in mitogenesis. *Progress in Biophysics and Molecular Biology* **59** 1–21. (https://doi.org/10.1016/0079-6107(93)90005-5)

Fliedner SM, Kaludercic N, Jiang XS, Hansikova H, Hajkova Z, Sladkova J, Limpuangthip A, Backlund PS, Wesley R, Martiniova L, *et al.* 2012 Warburg effect's manifestation in aggressive pheochromocytomas and paragangliomas: insights from a mouse cell model applied to human tumor tissue. *PLoS One* **7** e40949. (https://doi.org/10.1371/journal.pone.0040949)

Formigli L, Meacci E, Sassoli C, Squecco R, Nosi D, Chellini F, Naro F, Francini F & Zecchi-Orlandini S 2007 Cytoskeleton/stretch-activated ion channel interaction regulates myogenic differentiation of skeletal myoblasts. *Journal of Cellular Physiology* **211** 296–306. (https://doi.org/10.1002/jcp.20936)

Gao R, Yang T & Xu W 2017 Enemies or weapons in hands: investigational anti-diabetic drug glibenclamide and cancer risk. *Expert Opinion on Investigational Drugs* **26** 853–864. (https://doi.org/10.1080/13543784.2017.1333104)

Ghayee HK, Bhagwandin VJ, Stastny V, Click A, Ding LH, Mizrachi D, Zou YS, Chari R, Lam WL, Bachoo RM, *et al.* 2013 Progenitor cell line (hPheo1) derived from a human pheochromocytoma tumor. *PLoS One* **8** e65624. (https://doi.org/10.1371/journal.pone.0065624)

Haren N, Khorsi H, Faouzi M, Ahidouch A, Sevestre H & Ouadid-Ahidouch H 2010 Intermediate conductance Ca2+ activated K+ channels are expressed and functional in breast adenocarcinomas: correlation with tumour grade and metastasis status. *Histology and Histopathology* **25** 1247–1255. (https://doi.org/10.14670/HH-25.1247)

Jhawar S, Arakawa Y, Kumar S, Varghese D, Kim YS, Roper N, Elloumi F, Pommier Y, Pacak K & Del Rivero J 2022 New insights on the genetics of pheochromocytoma and paraganglioma and its clinical implications. *Cancers (Basel)* **14**. (https://doi.org/10.3390/cancers14030594)

Lenders JWM, Kerstens MN, Amar L, Prejbisz A, Robledo M, Taieb D, Pacak K, Crona J, Zelinka T, Mannelli M, *et al.* 2020 Genetics,

diagnosis, management and future directions of research of phaeochromocytoma and paraganglioma: a position statement and consensus of the Working Group on Endocrine Hypertension of the European Society of Hypertension. *Journal of Hypertension* **38** 1443–1456. (https://doi.org/10.1097/HJH.0000000000002438)

Livak KJ & Schmittgen TD 2001 Analysis of relative gene expression data using real-time quantitative PCR and the 2(-Delta Delta C(T)) Method. *Methods* **25** 402–408. (https://doi.org/10.1006/meth.2001.1262)

Loriot C, Burnichon N, Gadessaud N, Vescovo L, Amar L, Libé R, Bertherat J, Plouin PF, Jeunemaitre X, Gimenez-Roqueplo AP, *et al.* 2012 Epithelial to mesenchymal transition is activated in metastatic pheochromocytomas and paragangliomas caused by SDHB gene mutations. *Journal of Clinical Endocrinology and Metabolism* **97** E954–E962. (https://doi.org/10.1210/jc.2011-3437)

Loriot C, Domingues M, Berger A, Menara M, Ruel M, Morin A, Castro-Vega LJ, Letouzé É, Martinelli C, Bemelmans AP, *et al.* 2015 Deciphering the molecular basis of invasiveness in Sdhb-deficient cells. *Oncotarget* **6** 32955–32965. (https://doi.org/10.18632/oncotarget.5106)

Luciani P, Deledda C, Benvenuti S, Squecco R, Cellai I, Fibbi B, Marone IM, Giuliani C, Modi G, Francini F, *et al.* 2013 Exendin-4 induces cell adhesion and differentiation and counteracts the invasive potential of human neuroblastoma cells. *PLoS One* **8** e71716. (https://doi.org/10.1371/journal.pone.0071716)

MacFarlane SN & Sontheimer H 2000 Changes in ion channel expression accompany cell cycle progression of spinal cord astrocytes. *Glia* **30** 39–48. (https://doi.org/10.1002/(sici)1098-1136(200003)30:1<39::aid-glia5>3.0.co;2-s)

Malhi H, Irani AN, Rajvanshi P, Suadicani SO, Spray DC, McDonald TV & Gupta S 2000 KATP channels regulate mitogenically induced proliferation in primary rat hepatocytes and human liver cell lines. Implications for liver growth control and potential therapeutic targeting. *Journal of Biological Chemistry* **275** 26050–26057. (https://doi.org/10.1074/jbc.M001576200)

Maqoud F, Scala R, Hoxha M, Zappacosta B & Tricarico D 2022 ATP-sensitive potassium channel subunits in neuroinflammation: novel drug targets in neurodegenerative disorders. *CNS and Neurological Disorders Drug Targets* **21** 130–149. (https://doi.org/10.2174/1871527320666210119095626)

Martinelli S, Riverso M, Mello T, Amore F, Parri M, Simeone I, Mannelli M, Maggi M & Rapizzi E 2022 SDHB and SDHD silenced pheochromocytoma spheroids respond differently to tumour microenvironment and their aggressiveness is inhibited by impairing stroma metabolism. *Molecular and Cellular Endocrinology* **547** 111594. (https://doi.org/10.1016/j.mce.2022.111594)

Matlac DM, Hadrava Vanova K, Bechmann N, Richter S, Folberth J, Ghayee HK, Ge GB, Abunimer L, Wesley R, Aherrahrou R, *et al.* 2021 Succinate mediates tumorigenic effects via Succinate Receptor 1: Potential for New Targeted Treatment Strategies in Succinate Dehydrogenase Deficient Paragangliomas. *Frontiers in Endocrinology (Lausanne)* **12** 589451. (https://doi.org/10.3389/fendo.2021.589451)

Morata-Tarifa C, Jiménez G, García MA, Entrena JM, Griñán-Lisón C, Aguilera M, Picon-Ruiz M & Marchal JA 2016 Low adherent cancer cell subpopulations are enriched in tumorigenic and metastatic epithelial-to-mesenchymal transition-induced cancer stem-like cells. *Scientific Reports* **6** 18772. (https://doi.org/10.1038/srep18772)

Nichols CG 2006 KATP channels as molecular sensors of cellular metabolism. *Nature* **440** 470–476. (https://doi.org/10.1038/nature04711)

Ostroumov A, Simonetti M & Nistri A 2011 Cystic fibrosis transmembrane conductance regulator modulates synaptic chloride homeostasis in motoneurons of the rat spinal cord during neonatal development. *Developmental Neurobiology* **71** 253–268. (https://doi.org/10.1002/dneu.20855)

Pastushenko I & Blanpain C 2019 EMT transition states during tumor progression and metastasis. *Trends in Cell Biology* **29** 212–226. (https://doi.org/10.1016/j.tcb.2018.12.001)

Payne SL, Ram P, Srinivasan DH, Le TT, Levin M & Oudin MJ 2022 Potassium channel-driven bioelectric signalling regulates metastasis in triple-negative breast cancer. *EBiomedicine* **75** 103767. (https://doi.org/10.1016/j.ebiom.2021.103767)

Prakash SB & Abshire P 2008 Tracking cancer cell proliferation on a CMOS capacitance sensor chip. *Biosensors and Bioelectronics* **23** 1449–1457. (https://doi.org/10.1016/j.bios.2007.12.015).

Proks P, de Wet H & Ashcroft FM 2010 Activation of the K(ATP) channel by Mg-nucleotide interaction with SUR1. *Journal of General Physiology* **136** 389–405. (https://doi.org/10.1085/jgp.201010475)

Rao JU, Engelke UF, Rodenburg RJ, Wevers RA, Pacak K, Eisenhofer G, Qin N, Kusters B, Goudswaard AG, Lenders JW, *et al.* 2013 Genotype-specific abnormalities in mitochondrial function associate with distinct profiles of energy metabolism and catecholamine content in pheochromocytoma and paraganglioma. *Clinical Cancer Research* **19** 3787–3795. (https://doi.org/10.1158/1078-0432.CCR-12-3922)

Rapizzi E, Ercolino T, Fucci R, Zampetti B, Felici R, Guasti D, Morandi A, Giannoni E, Giaché V, Bani D, *et al.* 2014 Succinate dehydrogenase subunit B mutations modify human neuroblastoma cell metabolism and proliferation. *Hormones and Cancer* **5** 174–184. (https://doi.org/10.1007/s12672-014-0172-3)

Rapizzi E, Fucci R, Giannoni E, Canu L, Richter S, Cirri P & Mannelli M 2015 Role of microenvironment on neuroblastoma SK-N-AS SDHB-silenced cell metabolism and function. *Endocrine-Related Cancer* **22** 409–417. (https://doi.org/10.1530/ERC-14-0479)

Rhie DJ, Yi SY, Hahn SJ, Sim SS, Jo YH & Kim MS 1999 Somatostatin potentiates voltage-dependent K+ and Ca2+ channel expression induced by nerve growth factor in PC12 cells. *Brain Research. Developmental Brain Research* **112** 267–274. (https://doi.org/10.1016/s0165-3806(98)00175-8)

Richter S, Peitzsch M, Rapizzi E, Lenders JW, Qin N, de Cubas AA, Schiavi F, Rao JU, Beuschlein F, Quinkler M, *et al.* 2014 Krebs cycle metabolite profiling for identification and stratification of pheochromocytomas/paragangliomas due to succinate dehydrogenase deficiency. *Journal of Clinical Endocrinology and Metabolism* **99** 3903–3911. (https://doi.org/10.1210/jc.2014-2151)

Richter S, D'Antongiovanni V, Martinelli S, Bechmann N, Riverso M, Poitz DM, Pacak K, Eisenhofer G, Mannelli M & Rapizzi E 2018 Primary fibroblast co-culture stimulates growth and metabolism in Sdhb-impaired mouse pheochromocytoma MTT cells. *Cell and Tissue Research* **374** 473–485. (https://doi.org/10.1007/s00441-018-2907-x)

Rossitti HM, Dutta RK, Larsson C, Ghayee HK, Söderkvist P & Gimm O 2020 Activation of RAS signalling is associated with altered cell adhesion in phaeochromocytoma. *International Journal of Molecular Sciences* **21**. (https://doi.org/10.3390/ijms21218072)

Sbrana F, Sassoli C, Meacci E, Nosi D, Squecco R, Paternostro F, Tiribilli B, Zecchi-Orlandini S, Francini F & Formigli L 2008 Role for stress fiber contraction in surface tension development and stretch-activated channel regulation in C2C12 myoblasts. *American Journal of Physiology. Cell Physiology* **295** C160–C172. (https://doi.org/10.1152/ajpcell.00014.2008)

Shi X, Zhen L, Ding H, Chen J, Zhang S & Fu Y 2019 Role of ATP-sensitive potassium channels and inflammatory response of basilar artery smooth muscle cells in subarachnoid hemorrhage of rabbit and immune-modulation by shikonin. *Food and Chemical Toxicology* **134** 110804. (https://doi.org/10.1016/j.fct.2019.110804)

Squecco R, Chellini F, Idrizaj E, Tani A, Garella R, Pancani S, Pavan P, Bambi F, Zecchi-Orlandini S & Sassoli C 2020 Platelet-rich plasma modulates gap junction functionality and connexin 43 and 26 expression during TGF-β1-induced fibroblast to myofibroblast transition: clues for counteracting fibrosis. *Cells* **9**. (https://doi.org/10.3390/cells9051199)

Sundelacruz S, Levin M & Kaplan DL 2009 Role of membrane potential in the regulation of cell proliferation and differentiation. *Stem Cell Reviews and Reports* **5** 231–246. (https://doi.org/10.1007/s12015-009-9080-2)

Tabebi M, Kumar Dutta R, Skoglund C, Söderkvist P & Gimm O 2022 Loss of SDHB induces a metabolic switch in the hPheo1 cell line toward enhanced OXPHOS. *International Journal of Molecular Sciences* **23**. (https://doi.org/10.3390/ijms23010560)

Tretter L, Patocs A & Chinopoulos C 2016 Succinate, an intermediate in metabolism, signal transduction, ROS, hypoxia, and tumorigenesis. *Biochimica et Biophysica Acta* **1857** 1086–1101. (https://doi.org/10.1016/j.bbabio.2016.03.012)

Walia V & Elble RC 2010 Enrichment for breast cancer cells with stem/progenitor properties by differential adhesion. *Stem Cells and Development* **19** 1175–1182. (https://doi.org/10.1089/scd.2009.0430)

Wang Z, Bian W, Yan Y & Zhang DM 2022 Functional regulation of KATP Channels and Mutant Insight Into Clinical Therapeutic Strategies in Cardiovascular Diseases. *Frontiers in Pharmacology* **13** 868401. (https://doi.org/10.3389/fphar.2022.868401)

Warburg O, Wind F & Negelein E 1927 The metabolism of tumors in the body. *Journal of General Physiology* **8** 519–530. (https://doi.org/10.1085/jgp.8.6.519)

Wondergem R, Cregan M, Strickler L, Miller R & Suttles J 1998 Membrane potassium channels and human bladder tumor cells: II. Growth properties. *Journal of Membrane Biology* **161** 257–262. (https://doi.org/10.1007/s002329900332)

Yang M & Brackenbury WJ 2013 Membrane potential and cancer progression. *Frontiers in Physiology* **4** 185. (https://doi.org/10.3389/fphys.2013.00185)

Yasukagawa T, Niwa Y, Simizu S & Umezawa K 2012 Suppression of cellular invasion by glybenclamide through inhibited secretion of platelet-derived growth factor in ovarian clear cell carcinoma ES-2 cells. *FEBS Letters* **586** 1504–1509. (https://doi.org/10.1016/j.febslet.2012.04.007)

Zhao S, Wang M & Ma Z 2021 Therapeutic potential of ATP-sensitive potassium channels in Parkinson's disease. *Brain Research Bulletin* **169** 1–7. (https://doi.org/10.1016/j.brainresbull.2021.01.003)

Zhu YT, Wang CY, Pang SY, Lei CY, Luo Y & Tan WL 2018 A modified method by differential adhesion and serum-free culture medium for enrichment of cancer stem cells. *Journal of Cancer Research and Therapeutics* **14**(Supplement) S421–S426. (https://doi.org/10.4103/0973-1482.174533)

Received 5 June 2023
Accepted 25 July 2023
Available online 26 July 2023
Version of Record published 25 August 2023